Volcanic Cohesive Soil Behaviour under Static and Cyclic Loading

W. O. Sumartini[1], H. Hazarika[1], T. Kokusho[2], and S. Ishibashi[3]
[1]*Department of Civil Engineering, Kyushu University, Fukuoka, Japan*
[2]*Chuo University, Tokyo, Japan*
[3]*Department of Survey and Analysis, Nihon Chiken Co. Ltd., Fukuoka, Japan*
E-mail: waode_sumartini@yahoo.co.id

ABSTRACT: The objective of this study is to evaluate the behavior of reconstituted (disturbed) samples of volcanic soil under static and cyclic loading using a series of undrained static and cyclic tests. The static test results show that under low confining pressure, the disturbed sample is contracted and then dilated with no sign of temporary liquefaction. On the contrary, the undisturbed sample is dilated under low confining pressure and becomes contracted when reaching the peak of the soil strength. However, under high confining pressure, both disturbed and undisturbed samples show a contraction. The cyclic test results show cyclic mobility behavior under an investigated cyclic stress ratio. At a low cyclic stress ratio, the shear strain increases slowly, and after a certain number of cycles, the shear strain significantly increases. Conversely, the shear strain increases gradually at a high cyclic stress ratio. These results indicate a contradictive behavior of the soil under different confining stress and cyclic stress ratios.

KEYWORDS: Static triaxial test, Cyclic triaxial test, Volcanic soil, Reconstituted samples, Soil behavior

1. INTRODUCTION

Historically, in Japan, some damages triggered by an earthquake on volcanic soil areas have been reported. Earthquakes have been known to cause some damages to volcanic soil areas in Japan (Hazarika et al., 2017; Song et al., 2017; Kazama et al., 2012; Miyagi et al., 2011; Sassa, 2005). One of such area is Aso Caldera in the Kumamoto prefecture. This area suffered from widespread landslides which were triggered by the 2016 Kumamoto earthquake (Figure 1).

The landslides were concentrated in the Mount Aso area, within a 64 km radius of the epicenter. The 2016 Kumamoto earthquake refers to a series of earthquakes that struck the Kumamoto Prefecture of Kyushu Island on 14–16 April 2016. The foreshock earthquake occurred at 21.26 JST on 14 April 2016 at an epicentral depth of ~11 km and a magnitude (Mw) of 6.5. The mainshock struck at 01.25 JST on 16 April at an epicentral depth of ~10 km and Mw of 7 (USGS). The source of the earthquakes was the tectonic activity of the Hinagu and Futagawa faults (GSI). These two faults experienced more than 2 m of strike-slip displacement at shallow depth. One of the landslides occurred near the Aso Volcanological Laboratory of Kyoto University (Figure 2). This landslide brought damage to houses (Figure 3), public spaces, and roads (Figure 4). The inclination of the slope is about 10–15° Kochi et al. (2018) which is consistent with the value of 12° found by Song et al. (2017). Following those landslides, several volcanic soil deposits have been found scattered on the slopes. Sumartini et al. (2017) reported that the slope is composed of volcaniclastic deposits (Figure 5) which have different colors and characteristics. The volcanic soil deposits came from different places as listed in Table 1. Song et al. (2017) and Kochi et al. (2018) found that the landslide was composed of Kusasenrigahama pumice tephra beds (referred to as Orange soil in this paper). This Orange soil deposit, which acted as the slip surface of the landslide, is located on the top of the Pre Takanoobane Lava pumice deposit (referred to as Blackish soil). On one hand, from the map of resistivity distribution of the slope (Figure 6) that has been drawn by Kochi et al. (2018), it can be concluded that the Orange soil is in a saturated condition and it is located on the ground waterbed. However, the resistivity map also shows that the Blackish soil is an impermeable deposit. Based on these facts, the authors presume that the Orange soil deposit was liquefied during the earthquake and became the main reason for the occurrence of the landslide.

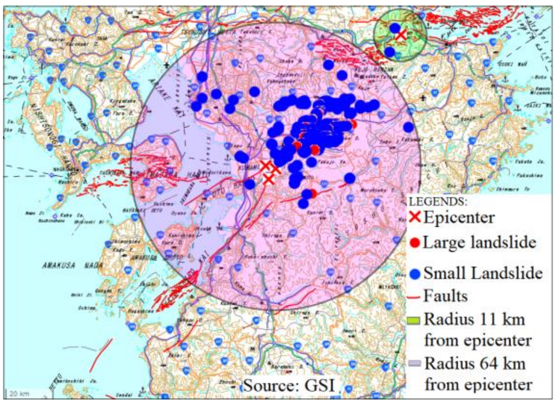

Figure 1 Map showing the landslide distribution by size within a 64 km radius of the Aso caldera (Sourced from GSI)

Figure 2 A massive landslide near the Aso Volcanological Laboratory of Kyoto University


Figure 3 Swept away houses

Several studies related to Orange soil were done and reported by Sumartini et al., (2017-2018). They studied chemical, mineral, and microstructure characteristics as well as the behavior of Orange soil under static and cyclic loading. According to these studies, the landslide occurred because the earthquake ruptured the soil structure of the Orange soil deposit and led to its liquefaction. Several researchers have studied the behavior of volcanic soils following earthquakes by conducting triaxial cyclic tests (Ishikawa and Miura in 2011, Suzuki and Yamamoto in 2004, Hatanaka et al. in 1985, and Sumartini et al. from 2017 to 2018). However, the behavior of the Orange soil under disturbed conditions has not been studied yet. For that reason, a series of undrained cyclic triaxial tests were performed to evaluate the behavior of disturbed samples under cyclic loading. Finally, the results were compared with the previous study and are presented in this paper.

Figure 4 Damage to roads

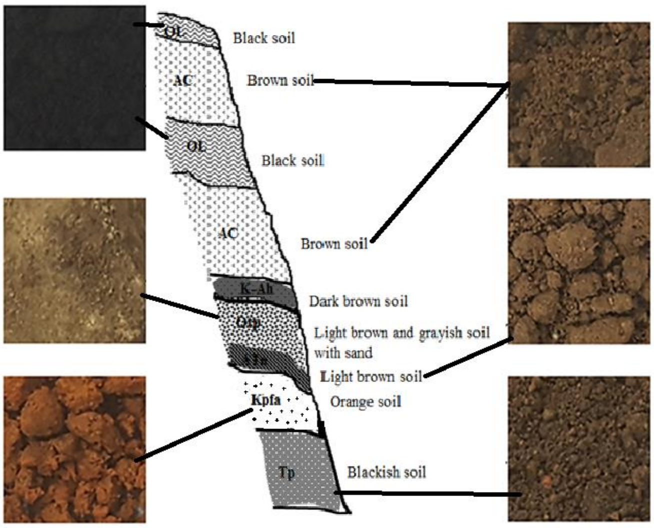

Figure 5 Schematic profile of the slope in Aso caldera (Modified from Sumartini et al. 2017)

Table 1 Origin of volcanic soil in Aso caldera (Kochi et al., 2018)

Deposit	Origin	Age (Cal ka)
Black soil	Organic (OL)	10-present
Brown soil	Aso Central Cone Pumice (AC)	7.3-10
Dark brown soil	Kikai Akahoya Ash (K-Ah)	7.3
Light brown and grayish soil with sand	Otogase Lava Pumice (Otp)	29-7.3
Light brown soil	Aira Tn (Atn)	29
Orange soil	Kusasenrigahama Pumice (Kpfa)	31
Blackish soil	Takanoobane Lava Pumice (Tp)	51±5

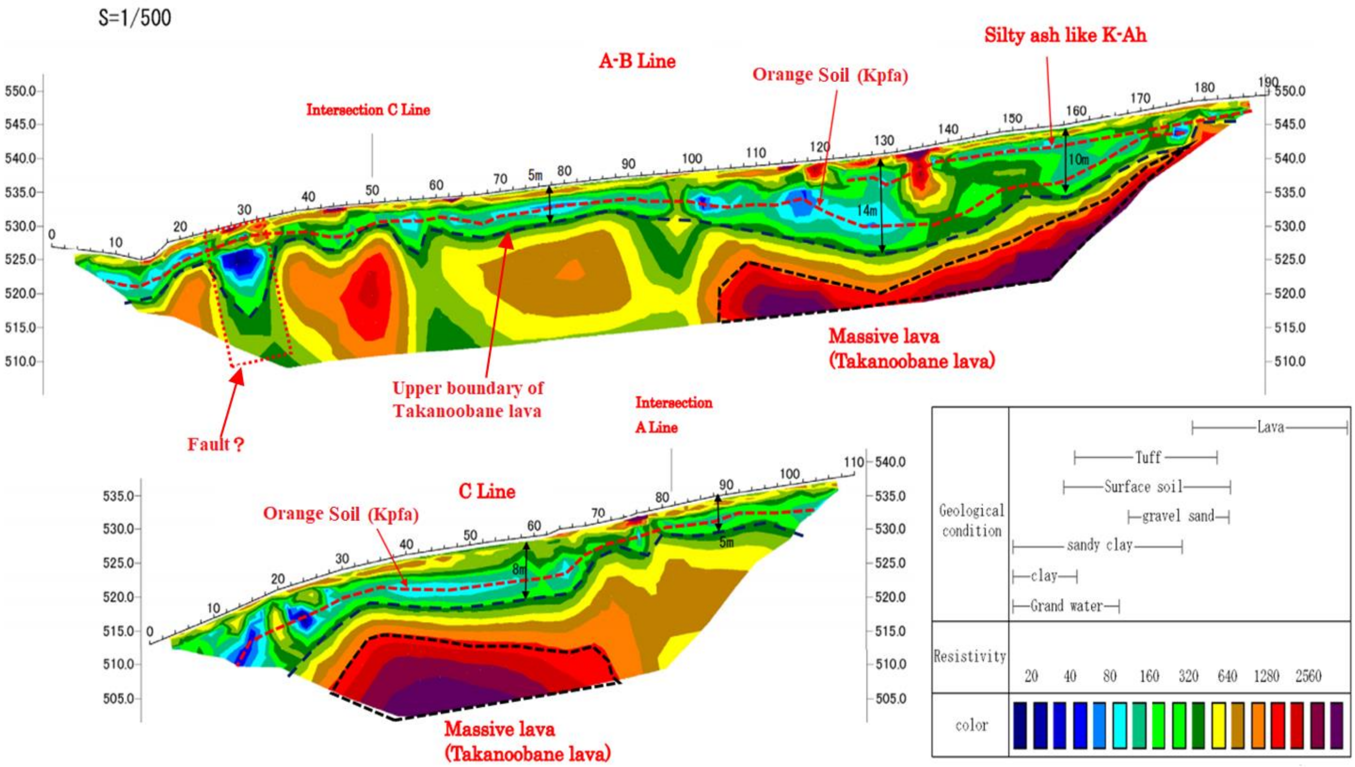

Figure 6 Resistivity distribution of the slope in Aso Volcanological Laboratory (Kochi et al., 2018)

2. MATERIAL PROPERTIES

The Orange soil is taken from the scarp of the slope near the Aso Volcanological Laboratory. This soil contains about 60 percent of fine particles (Figure 7), and based on its properties (Table 2), it can be classified as volcanic cohesive soil type II. It also contains 97 % of feldspar mineral by weight (Table 3) and has a vesicular fabric composed of crystal flakes (Figure 8). Sumartini et al. (2018b) idealized the flakes of the volcaniclastic deposit of the slope into flower type (Figure 9a) and petal-type (Figure 9b).

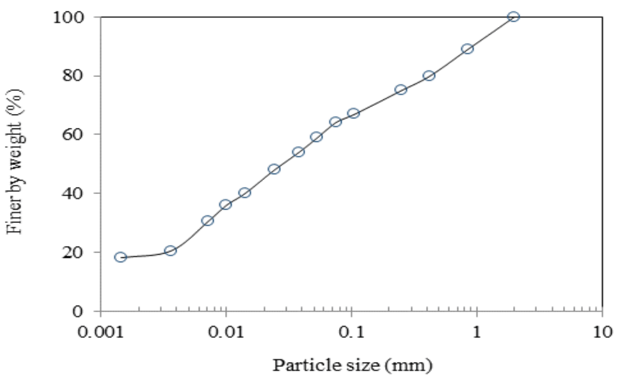

Figure 7 Grain size distribution of the Orange soil (Sumartini et al., 2017)

Table 2 Physical properties of Orange soil (Sumartini et al., 2017)

Physical Properties	**Orange Soil**
Specific Gravity	2.24-2.38
Dry Density, g/cm^3	0.51-0.58
Wet Density, g/cm^3	1.23-1.30
Water Content, %	54.62-58.36
Liquid Limit, %	113.40
Plastic Limit, %	88.25
Plasticity Index	25.15

Table 3 The mineral content of Orange soil (Sumartini et al., 2018[a])

Contents	**Orange soil (Percent by weight)**
Albite	57
Bytownite	40
Sodium hydrogen sulfide	2.0
Calcium copper germanium oxide	1.4

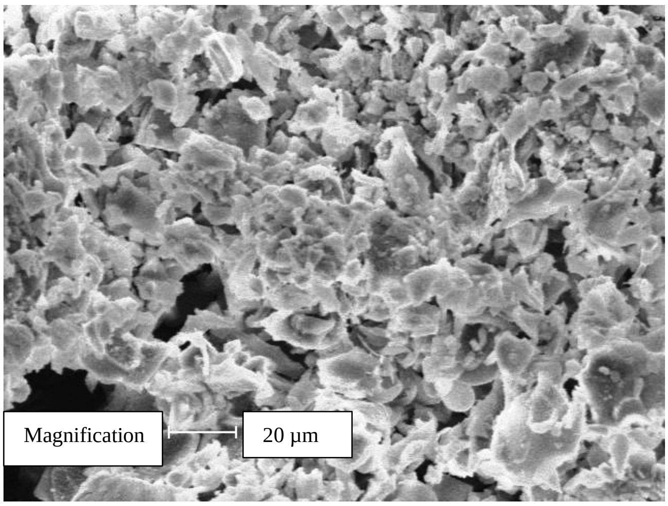

Figure 8 A vesicular structure of Orange Soil fabric (Sumartini et al., 2017)

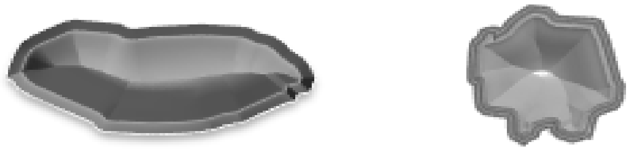

(a) Petal-type (b) Flower type

Figure 9 Idealized crystal flake structures found in the deposits of the Aso Volcanological Laboratory Landslide. a) Petal-type structure and b) Flower-type structure (Sumartini et al., 2018[b])

3. TESTING METHOD

The behavior of the soil under cyclic loading was measured by conducting the undrained triaxial test. The triaxial testing procedures are referred to as the Japanese Geotechnical Society Standard (JGS 0541-2009). In this test, reconstituted samples (hereafter called disturbed samples) were used. The disturbed samples were prepared by reconstituting the undisturbed samples which were subjected to cyclic loading. The average dry density of these samples is similar to undisturbed samples. They were reconstituted using a steel mold 100 mm in height and 50 mm in diameter. The sample was fully saturated (Skempton's B value higher than 0.95) by circulating carbon dioxide gas followed by de-aired water using the double vacuuming method. Then, the sample was consolidated isotropically to an effective confining pressure of 60 kPa, cell pressure $\sigma_c = 160$ kPa, and water pressure $u_w = 100$ kPa. The effective confining pressure was adequate for the field condition. After the isotropic consolidation, the samples were subjected to a vertical load cycles with a doubled amplitude vertical strain of about 10%. The frequency of the cyclic axial load was 0.1 Hz. The test was conducted on disturbed samples by applying 0.260, 0.268, 0.356, and 0.402 of cyclic stress ratio $\sigma_d/2\sigma'_c$. The applied cyclic stress ratio (CSR) in this study was lower compared to the study previously conducted by Sumartini et al. (2018[a]). The disturbed sample was expected to be weaker in liquefaction resistance compared to the undisturbed sample. To decide whether liquefaction occurred in this study or not, the pore water pressure ratio (r_u) was used, defined as the ratio of the pore water pressure to the normal stress. When $r_u \geq 0.95$, the specimen was considered to have liquefied. The results of this test were compared to the behavior of the undisturbed sample under static and cyclic loading from the previous research done by Sumartini et al. (2018[a]).

4. RESULTS AND DISCUSSION

4.1 Soil behavior under static loading

Figures 10 and 11 show the stress-strain relationship of undisturbed and disturbed samples, respectively, in undrained static triaxial tests. The two figures show that under high confining pressure the samples tend to reach the peak deviator stress under a small amount of strain. Conversely, under low confining pressure, the samples tend to reach the peak deviator stress under a large amount of strain. For undisturbed samples, under the investigated confining stress, the deviatoric stress increases gradually with the progress of axial strain. However, when the undisturbed samples reach the peak of a specific strain, the deviatoric stress decreases significantly until it reaches a certain amount of strain. Then the deviator stress decreases steadily along with the strain. This behavior is classified as a strain-softening behavior. Conversely, the orange soil shows an elastic-perfectly plastic behavior for disturbed samples under a high confining pressure (120 kPa and 240 kPa). The deviatoric stress also rises gradually with the progress of axial strain for each confining pressure but when it reaches the peak, the stress decreases steadily. At a low confining pressure (60 kPa), the disturbed sample shows a strain hardening behavior. The deviator stress increases linearly and reaches an initial yield strength under a small amount of strain, then the deviator stress increases again until it reaches the ultimate strength under a large amount strain.

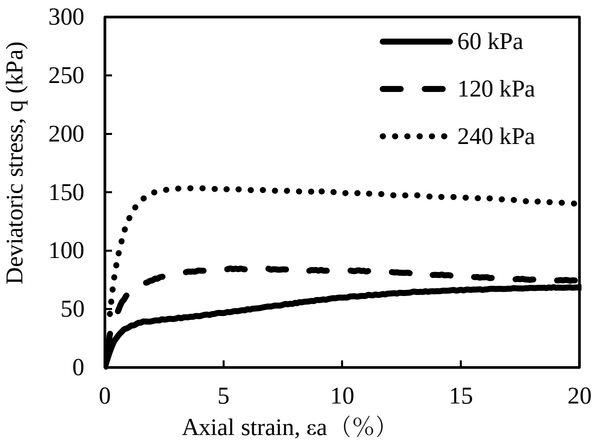

Figure 10 Stress versus axial strain of disturbed samples (Sumartini et al., 2018[a])

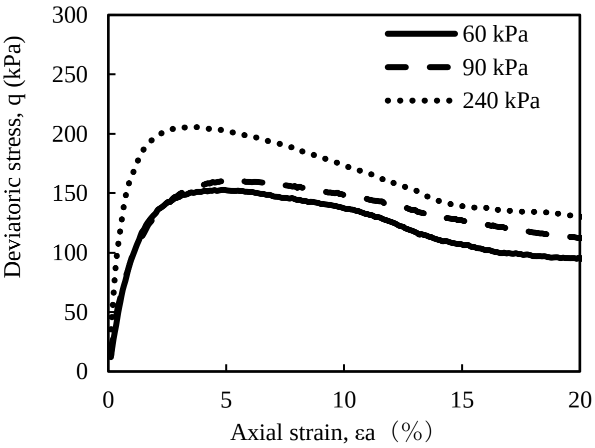

Figure 11 Stress versus axial strain of undisturbed samples (Sumartini et al., 2018[a])

Figures 12 and 13 show the pore water pressure-strain relationship of undisturbed and disturbed samples, respectively, in undrained static triaxial tests. The two figures show that under high confining pressure the samples tend to reach the peak of pore water pressure under a large amount of strain. Conversely, under low confining pressure, the samples tend to reach the peak of pore water pressure under a small amount of strain. For undisturbed samples, under low confining pressure, the pore water pressure increases linearly with the progress of axial strain, but when it reaches the peak of a specific strain, the pore water pressure decreases significantly until it reaches a certain amount of strain. It then increases steadily along with the strain. This behavior could occur due to the brittleness of the soil material. Under high confining pressure, the pore water pressure tends to increase linearly until it reaches a certain amount of strain. Then, it starts to increase steadily along with the axial strain. This behavior is also found in the disturbed samples, under high confining pressure (120 kPa and 240 kPa). At low confining pressure (60 kPa), the disturbed sample shows that the pore water pressure increases linearly with the progress of axial strain, but when it reaches the peak, the pore water pressure then decreases steadily along with the amount of strain.

The soil liquefaction vulnerability can be projected by plotting the pore water pressure ratio ($r_u=u/\sigma c$) vs strain behavior as shown in Figure 14. For all investigated samples, it can be noted that the r_u under low confining pressure is significantly higher than under high confining pressure, meaning that soil in shallow depths is more vulnerable to liquefaction. By comparing the r_u-strain behavior between undisturbed and disturbed samples, it is found that the soil fabric only has a significant effect on liquefaction vulnerability for soil under low confining pressure.

The behavior of the undisturbed and disturbed samples can be clarified by looking at the stress path of the soil as shown in Figure 15. The undisturbed sample is dilated under low confining pressure and becomes contracted when reaching the peak of the soil strength. This behavior is a sign of soil brittleness. Under high confining pressure, the undisturbed samples show a contractive behavior. This contractive behavior was also found in disturbed samples. Under low confining pressure, the disturbed sample is contracted and then dilated with no sign of temporary liquefaction. The meeting of the endpoints between the dilative curve (60 kPa of confining pressure) and the contractive curve (120 kPa of confining pressure) of the disturbed soil (in the coordinate of 68,74 kPa of deviator stress and 45.11 kPa of mean effective stress) is defined as the steady-state point of the orange soil. The phase transformation line is made by drawing a line between the endpoints of the dilative curve and the contractive curve. The flow liquefaction surface is defined by connecting the peak of the disturbed samples curve up to the steady-state point. The zone located on the right side of the flow liquefaction surface and above the steady-state point is called the flow liquefaction susceptible zone. The zone that is located on the right side of the phase transformation line and below the steady-state point is called the cyclic mobility susceptible zone. From the stress path curve, it can be noted that the behavior of the orange soil in undisturbed and disturbed samples under low confining pressure is completely different. Since the disturbed samples could not represent the behavior of undisturbed samples, it is not recommended to use the disturbed sample test results for an experiment design involving samples from a shallow depth.

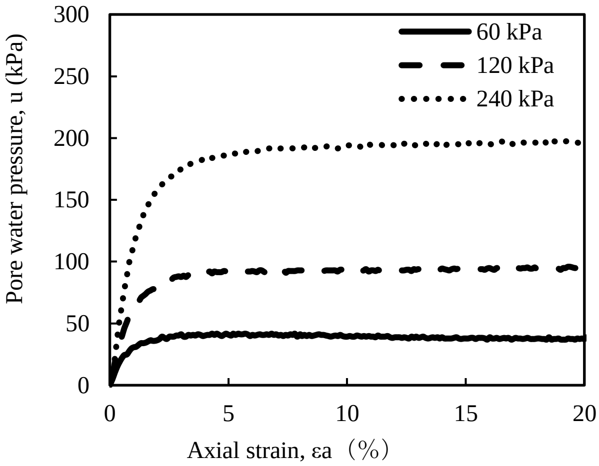

Figure 12 The Pore water pressure versus the axial strain of disturbed samples (Sumartini et al., 2018[a])

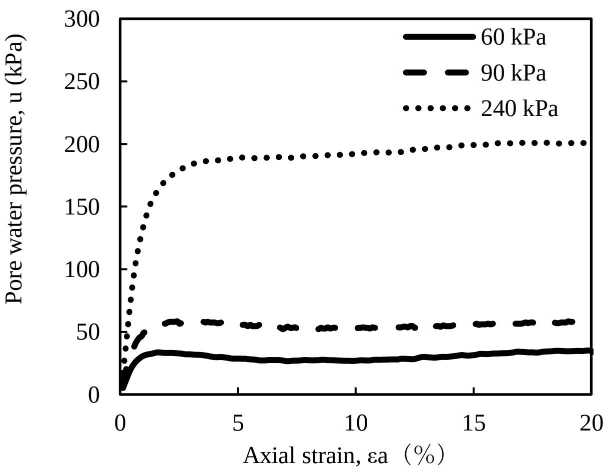

Figure 13 Pore water pressure versus the axial strain of undisturbed samples (Sumartini et al., 2018[a])

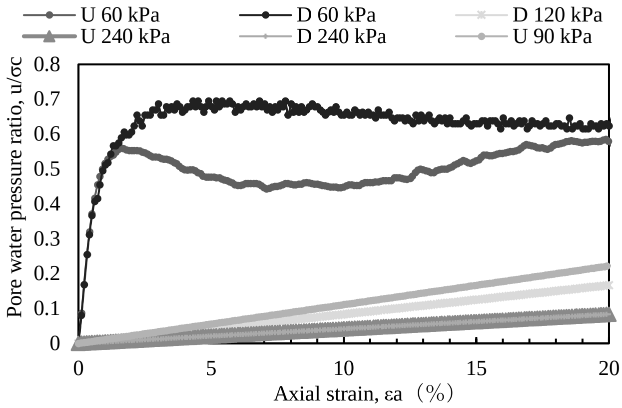

Figure 14 The pore water pressure ratio versus the axial strain of undisturbed and disturbed samples

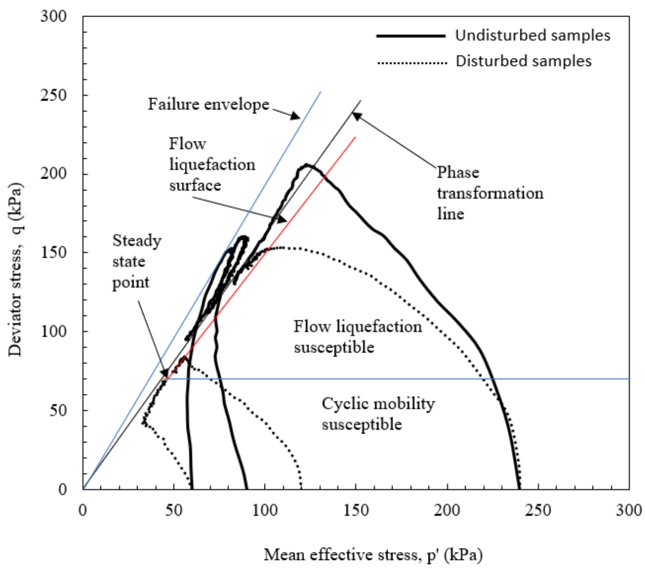

Figure 15 Stress path behavior of orange soil

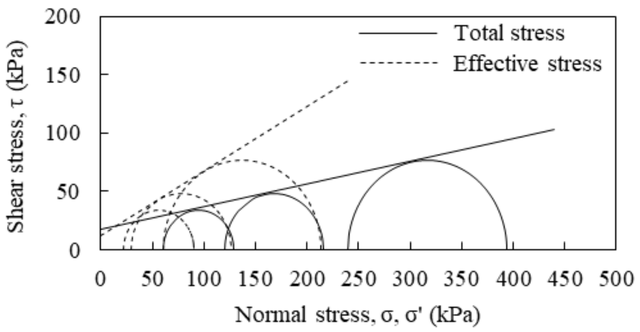

Figure 16 Mohr's Circle of disturbed samples

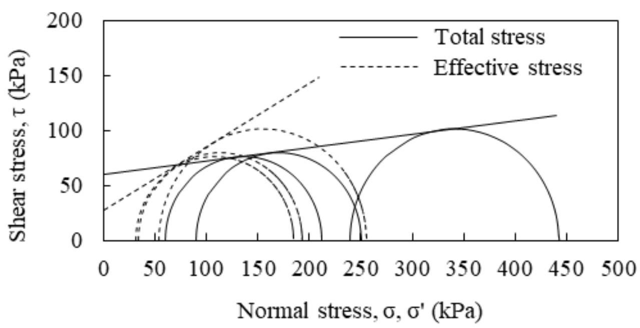

Figure 17 Mohr's Circle of undisturbed samples

Table 4 Strength parameter of the Orange soil

Strength parameter	Disturbed	Undisturbed
C_{cu} (kPa)	17	60
φ (°)	11	7
c' (kPa)	11.5	27.5
φ' (°)	29	30

Figures 16 and 17 show the Mohr's stress circle of undisturbed and disturbed samples separately. The cohesion and angle of the shear strength of total stress and effective stress are listed in Table 4. It shows that the orange soil has a considerably high cohesivity regardless of the condition of the samples which confirmed the classification of the soil based on its physical properties. For undisturbed samples, the cohesion of effective stress is about 2.18 times the total stress while the angle is about 0.23 times the total stress. For disturbed samples, the cohesion of effective stress is about 1.48 times the total stress, and the angle is about 0.34 times the total stress. Finally, by comparing the cohesion and the angle of both samples, it can be concluded that the reconstitution process reduces cohesion by about 3.53 times for total stress and about 2.40 times for effective stress while increasing the angle about 1.57 times for both total stress and effective stress.

4.2 Soil behavior under cyclic loading

Figure 18 shows the typical response of disturbed samples in the undrained cyclic triaxial test. It shows that the effective stress decreases along with the number of cycles. Contrastingly, the pore water pressure ratio and the strain increase along with the number of cycles. For simplification purposes, the behavior of disturbed and undisturbed samples (Sumartini et al., 2018[a]) on effective stress, pore water pressure ratio (r_u), and double amplitude strain (DA) is presented in the maximum value of each cycle.

Figures 19 and 20 show the number of cycles as a function of the effective stress reduction of disturbed and undisturbed samples, respectively. The number required to reduce the effective stress decreases consistently with the magnitude of CSR and the reduction of effective stress for some samples is not close to zero. The effect of the reconstitution of soil structure on the effective stress behavior of orange soil can be seen by comparing the undisturbed sample with a CSR of 0.274 to the disturbed sample with a CSR of 0.268. Despite being higher in CSR, the undisturbed sample took about 153 cycles to reduce the effective stress to 20 kPa, while the disturbed sample only took about 10 cycles. From this it can be deduced that the change of soil structure due to reconstitution significantly decreases the ability of the soil to prevent the reduction of effective stress.

Figures 21 and 22 show the number of cycles as a function of DA of disturbed and undisturbed samples, respectively. The number required to reach the DA increases consistently with the magnitude of CSR. Additionally, all samples reach 5% of DA. The strain of most samples is generated incrementally along with the number of cycles, called cyclic mobility behavior. One exception is the undisturbed sample with a CSR of 0.735 which had a strain that rapidly generated flow type failure. The summary of the number of cycles required to reach 5% of DA is plotted in Figure 23. It shows that to cause liquefaction in 20 cycles, the disturbed sample requires a CSR of 0.265 and the undisturbed sample requires a CSR of 0.505, which is about two times higher than disturbed samples. Thus, it can be deduced that the reconstitution of soil structure significantly increases the ability of the soil to generate strain.

Figures 24 and 25 show the number of cycles as a function of r_u of disturbed and undisturbed samples, respectively. It can be noted that all the samples reach an r_u of 0.95 except the undisturbed sample with a CSR of 0.735, which failed at an r_u of 0.7. Additionally, the number required to initiate liquefaction for samples with smaller CSR is higher than samples with high CSR. By comparing the specimen with a CSR of 0.735 to the results of static loading with the same confining pressure, it can be seen that the peak r_u is about 0.7. Thus, results from the triaxial static test can be used for predicting the required pore water pressure ratio to cause flow liquefaction. The summary of the number of cycles required to reach an r_u of 0.95 is plotted in Figure 26. It shows that to cause liquefaction in 20 cycles, the disturbed sample required a CSR of 0.265 and the undisturbed sample required a CSR of 0.485, which is about two times higher than that of the disturbed samples. Thus, it can be deduced that the reconstitution of soil structure significantly increases the soil's ability to generate the excess pore water pressure ratio.

By comparing Figures 23 and 26, it can be noted that the required CSR to initiate liquefaction at 20 cycles for disturbed samples is similar in terms of 5% of DA and an r_u of 0.95. However, for undisturbed samples, the required CSR to initiate liquefaction in terms of 5% of DA is higher than in term of 0.95 of r_u. Thus, it can be deduced that landslides occur due to the liquefaction that is initiated by the increase of pore water pressure during the earthquake which is followed by the deformation of the slope.

By projecting the results with the stress path graph from undrained static triaxial tests (Figure 15), the liquefaction susceptibility type is confirmed. The zone that is located on the right side of the flow liquefaction surface and the deviator stress and is higher than the steady-state (68.74 kPa) is called the flow liquefaction susceptible zone. The zone that is located on the right side of the phase transformation line and the deviator stress and is lower than the steady-state is called the cyclic mobility susceptible zone. Therefore, all samples with a CSR of less than 0.573 (68.74 kPa/(2x60 kPa) are classified as cyclic mobility susceptibility. The prediction of the liquefaction type from the undrained static triaxial tests is similar to the results of undrained cyclic triaxial tests. Thus, it can be conceded that the stress path graph from the undrained static triaxial tests can be used for predicting the required CSR to cause liquefaction in the orange soil.

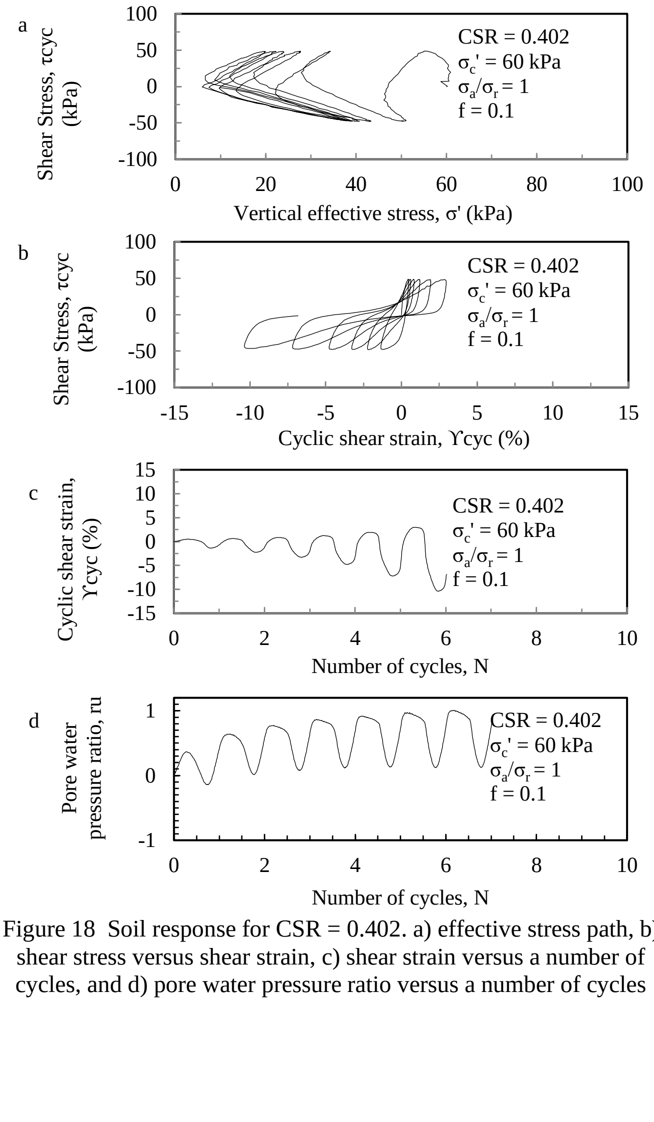

Figure 18 Soil response for CSR = 0.402. a) effective stress path, b) shear stress versus shear strain, c) shear strain versus a number of cycles, and d) pore water pressure ratio versus a number of cycles

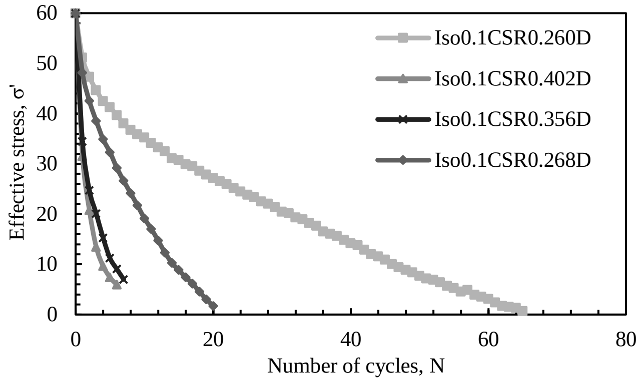

Figure 19 Effective stress for each cyclic loading of disturbed samples

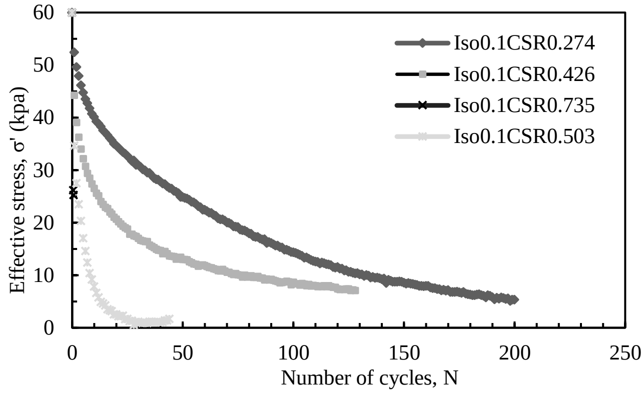

Figure 20 Effective stress for each cyclic loading of undisturbed samples (modified from Sumartini et al., 2018[a])

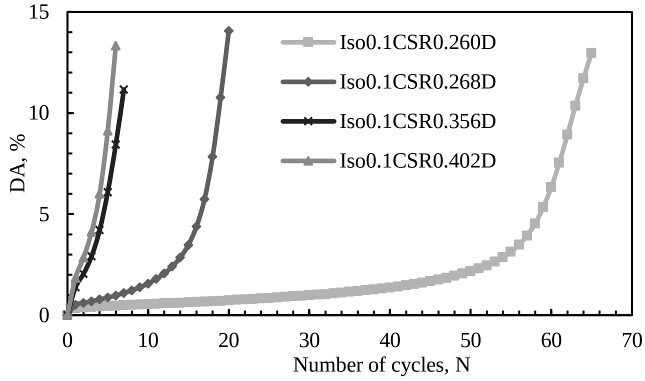

Figure 21 Double amplitude strain for each cyclic loading of disturbed samples

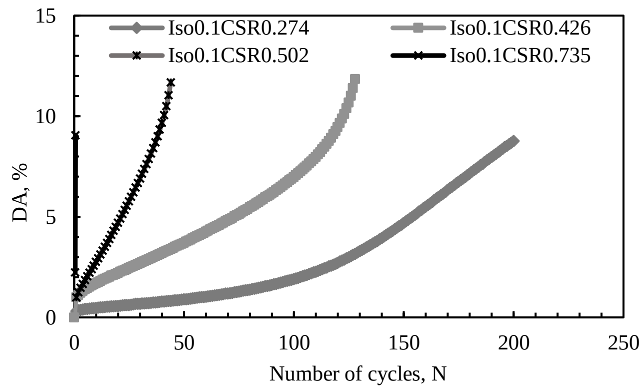

Figure 22 Double amplitude strain for each cyclic loading of undisturbed samples (modified from Sumartini et al., 2018[a])

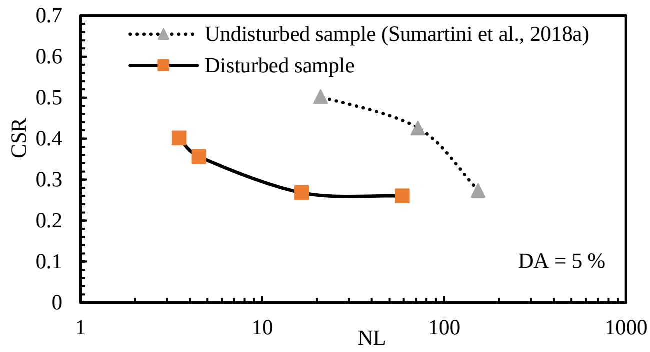

Figure 23 Liquefaction resistance of orange soil in terms of DA = 5%

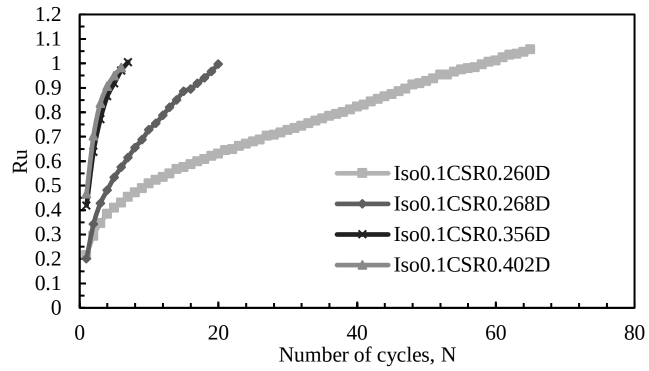

Figure 24 Excess pore water pressure ratio for each cyclic loading of disturbed samples

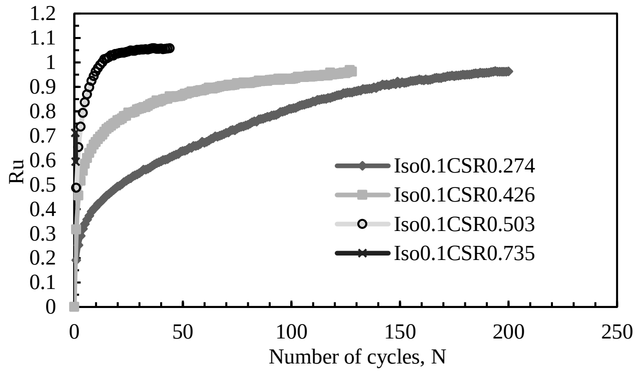

Figure 25 Excess pore water pressure ratio for each cyclic loading of undisturbed samples (modified from Sumartini et al., 2018[a])

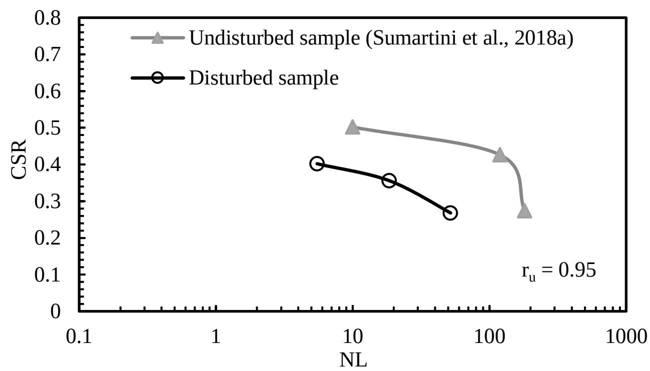

Figure 26 Liquefaction resistance of orange soil in terms of r_u = 0.95

4.3 Effect of cyclic loading on soil fabric

Figures 27 and 28, respectively, show the results of the SEM analysis of the orange soil structure before and after the liquefaction tests (Sumartini et al., 2018[a]). Figure 27 shows that the soil structure is composed of a stack of crystal flakes and is highly porous. In comparison, Figure 28 shows that the soil structure is visibly broken and has a reduced crystal flake size. Consequently, the number of small flakes in the soil fabric increases.

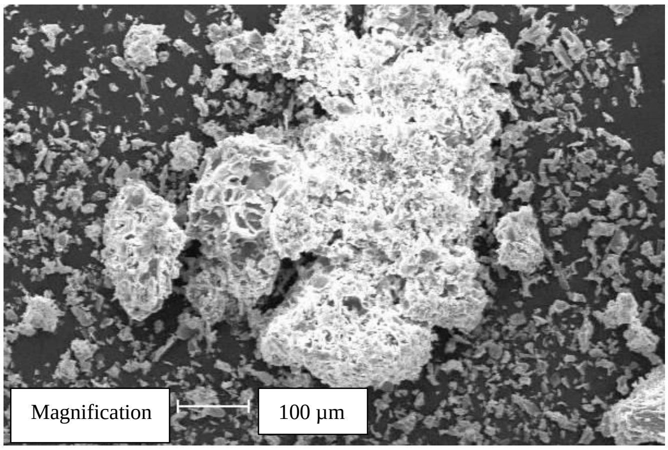

Figure 27 Soil structure state before cyclic loading (Sumartini et al. 2018[a])

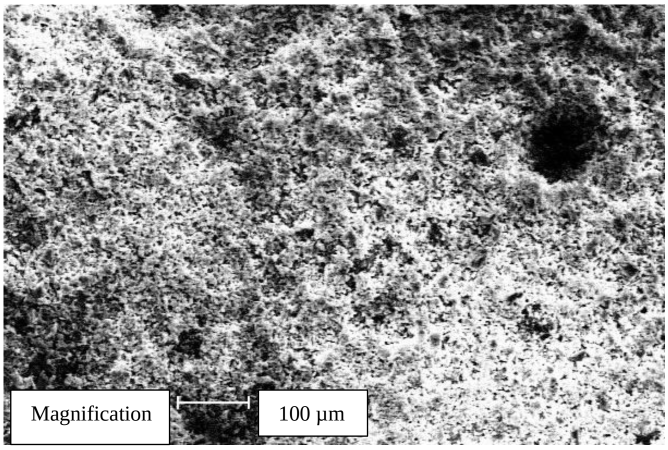

Figure 28 Soil structure state after cyclic loading (Sumartini et al. 2018[a])

5. CONCLUSIONS

From the results of the investigation, the following conclusions can be made:

1) The cohesion of the disturbed sample is significantly lower than the undisturbed sample because the bonding between the grains of the disturbed sample was broken due to the reconstitution process.
2) The behavior of the disturbed samples under low confining pressure is opposite that of the undisturbed samples. However, for high confining pressure, the behavior is similar. The strength of the soil in high confining pressure was higher than that in the lower confining pressure. As a result, it can be concluded that an orange soil deposit in a shallow depth is more susceptible to liquefaction than in a deep depth.
3) Under cyclic loading, both samples show cyclic mobility behavior under the amounts of CSR that were investigated except the undisturbed samples with a CSR of 0.735, which showed a flow liquefaction behavior.
4) The change of soil structure due to reconstitution significantly decreases the soil's ability to prevent the reduction of effective stress and increases the soil's ability to generate strain and the pore water pressure ratio, which reduces the liquefaction resistance of soil.

5) The cyclic loading affects the deformation of the soil fabric as confirmed by the reduction of the crystal flakes as seen in the SEM analysis.
6) The static and cyclic loading test along with the SEM test results suggest that the landslide occurred due to the mainshock. Even though the foreshock caused damage to the soil structure of the orange soil deposits, due to the high resistance of the orange soil deposit against liquefaction, the foreshock was not strong enough to trigger the landslide.

6. ACKNOWLEDGMENT

The financial grant for this research under the J-RAPID program (Principal Investigator: Hemanta Hazarika) of the Japan Science and Technology Agency (JST) is gratefully acknowledged. The first author is grateful to the Indonesia Endowment Fund for Education (LPDP) for financially supporting her study.

7. REFERENCES

Hatanaka, M., Sugimoto, M., and Suzuki, Y. (1985) "Liquefaction Resistance of Two Alluvial Volcanic Soils Sampled by In Situ Freezing", Soils and Foundations, 25, pp49-63.

Hazarika, H., Kokusho, T., Kayen, R.E., Dashti, S., Fukuoka, H., Ishizawa, T., Kochi, Y., Matsumoto, D., Hirose, T., Furuichi, H., Fujishiro, T., Okamoto, K., Tajiri, M., and Fukuda, M. (2017) "Geotechnical Damage due to the 2016 Kumamoto Earthquake and Future Challenges", Lowland Technology International, Special Issue on Kumamoto Earthquake and Disasters, 19, pp189-204.

Ishikawa, T., and Miura, S. (2011) "Influence of Freeze-Thaw Action on Deformation-Strength Characteristics and Particle Crushability of Volcanic Coarse-Grained Soils", Soils and Foundations, 51, pp785-799.

Kazama, M., Kataoka, S., and Uzuoka, R. (2012) "Volcanic Mountain Area Disaster Caused by the Iwate-Miyagi Nairiku Earthquake of 2008", Japan. Soil and Foundations, 52, pp168-184.

Kochi, Y., Kariya, T., Matsumoto, D., Hirose, T., and Hazarika, H. (2018) "Investigation of Slopes on the Takanoobane Lava Dome Using Resistivity Imaging Method", Lowland Technology International, Special Issue on Kumamoto Earthquake and Disasters, 19, pp261-266.

Miyagi, T., Higaki, D., Yagi, H., Yoshida, S., Chiba, N., Umemura, J., and Satoh, G. (2011) "Reconnaissance Report on Landslide Disaster in Northeast following the M 9 Tohoku Earthquake", Landslides, 8, pp339-342.

Sassa. K. (2005) "Landslide Disasters Triggered by the 2004 Mid-Niigata Prefecture Earthquake in Japan", Landslides, 4, pp113-122.

Song, K., Wang, F., Dai, Z., Iio, A., Osaka, O., and Sakata, S. (2017) "Geological Characteristics of Landslides Triggered by the 2016 Kumamoto Earthquake in Mt. Aso Volcano, Japan", Bulletin of Engineering Geology and the Environment, Springer-Verlag, pp1-10.

[a]Sumartini, W. O., Hazarika, H., Kokusho, T., Ishibashi, S., Matsumoto, D., and Chaudhary, B. (2018) "Deformation and Failure Characteristics of Volcanic Soil at Landslide Sites due to the 2016 Kumamoto Earthquake", Lowland Technology International, Special Issue on Kumamoto Earthquake and Disasters, 19, March 2018, pp237-244.

[b]Sumartini, W. O., Hazarika, H., Kokusho, T., Ishibashi, S., Matsumoto, D., and Chaudhary, B., (2018) "Microstructural Characteristics of Volcanic Soil in Aso Caldera related to the Landslide Triggered by the 2016 Kumamoto Earthquake", Proceedings of 16th European Conference on Earthquake Engineering, Thessaloniki, USB stick.

Sumartini, W. O., Hazarika, H., Kokusho, T., Ishibashi, S., Matsumoto, D., and Chaudhary, B., (2017) "Liquefaction Susceptibility of Volcanic Soil in Aso Caldera due to the 2016 Kumamoto Earthquake", Proceedings of the 19th International Summer Symposium, Fukuoka, pp13-14.

Suzuki, M., and Yamamoto, T., (2004) "Liquefaction Characteristic of Undisturbed Volcanic Soil in Cyclic Triaxial Test", Proceedings of 13th World Conference on Earthquake Engineering, Vancouver, Paper No. 465.